Spatial structure of neutron Cooper pair in low density uniform matter

Masayuki Matsuo*
Department of Physics, Faculty of Science, Niigata University, Niigata 950-2181, Japan
(Received 1 December 2005; published 13 April 2006)

The spatial structure of the neutron Cooper pair in superfluid low-density uniform matter is analyzed by means of BCS calculations employing a bare force and the effective Gogny interaction. It is shown that the Cooper pair exhibits a strong spatial dineutron correlation over a wide range of neutron densities $\rho/\rho_0 \approx 10^{-4} - 0.5$. This feature is related to the crossover behavior between the pairing of the weak coupling BCS type and the Bose-Einstein condensation of bound neutron pairs. It is also shown that the zero-range δ interaction can describe the spatial structure of the neutron Cooper pair if the density-dependent interaction strength and the cutoff energy are appropriately chosen. Parametrizations of the density-dependent δ interaction satisfying this condition are discussed.

DOI: 10.1103/PhysRevC.73.044309 PACS number(s): 21.60.Jz, 21.65.+f, 26.60.+c

I. INTRODUCTION

The importance of the pair correlation has been widely recognized for nucleon many-body systems in various circumstances, in particular in open-shell nuclei and in neutron stars. The pairing gap varies with system parameters such as N, Z, and the rotational frequency in the case of finite nuclei, or the temperature and the density in the case of neutron stars (cf. Refs. [1–5] as reviews). The pairing correlation at low nucleon density is of special interest, since the theoretical predictions for low-density uniform matter suggest that the pairing gap may take, at around 1/10 of the normal nuclear density, a value that is considerably larger than that at the normal density [3–5]. This feature is expected to have direct relevance to the properties of neutron stars, especially those associated with the inner crust [6,7]. The strong pairing at low density may also be relevant to finite nuclei, if one considers neutron-rich nuclei near the drip line [8–11]. This is because such nuclei often accompany an unsaturated low-density distribution of neutrons (the neutron skin and/or the neutron halo) surrounding the nuclear surface [12–14]. It is interesting to clarify how the pair correlation in these exotic nuclei is different from that in stable nuclei, reflecting the strong density dependence mentioned above. In this connection one would like to ask how the pair correlation at low nucleon density is different from that around the normal density.

The spatial structure of the neutron Cooper pair is focused on as a characteristic feature of low-density nucleon pairing. Its possible indication could be the dineutron correlation in the two-neutron halo nuclei, e.g., ^{11}Li, for which a spatially correlated pair formed by the halo neutrons has been predicted theoretically [8,15–20] and debated in experimental studies [21–24]. Further, a recent theoretical analysis [25] using the Hartree-Fock-Bogoliubov (HFB) method [26–29] also predicts the presence of a similar dineutron correlation in medium-mass neutron-rich nuclei where more than two weakly bound neutrons contribute to form the neutron skin in the exterior of the nuclear surface. It is also possible to argue the importance of the spatial correlation from a more fundamental viewpoint based on the nucleon interaction in the ^1S channel. The bare nucleon-nucleon interaction in this channel has a virtual state around zero energy, characterized by the large scattering length $a \approx -18$ fm, which implies a very strong attraction between a pair of neutrons with the spin singlet configuration. A rather general argument [30,31], which applies to a dilute limit of any Fermion system, indicates that the pair correlation of the Fermions interacting with a large scattering length differs significantly from what is considered in the conventional BCS theory [32] assuming weak coupling: it is then appropriate to consider a crossover between a superfluid system of the weak-coupling BCS type and a Bose-Einstein condensate of spatially compact bound Fermion pairs [30,31,33–35]. This BCS-BEC crossover phenomenon was recently observed in an ultracold atomic gas in a trap, for which the interaction is controllable [36]. In the case of the nucleon pairing, the BCS-BEC crossover has been argued mostly for the neutron-proton pairing in the $^3SD_1$ channel, for which the strong spatial correlation associated with the deuteron and the BEC of the deuterons may emerge [37–41]. Concerning the neutron pairing in the ^1S channel, which is discussed in the present paper, we may also expect that the strong coupling feature may lead to the spatial dineutron correlation, although the realization of the crossover could be marginal and should depend on the density [38].

In the present paper I would like to clarify how the spatial structure of the neutron Cooper pair varies with the density. For this purpose, I shall investigate the neutron pair correlation in symmetric nuclear matter and in neutron matter in the low-density region. Uniform matter is, of course, a simplification of the actual nucleon configurations in finite nuclei and neutron stars. However, it has a great advantage, as one can solve the gap equation in this case without ambiguity for various interactions including the bare nucleon-nucleon forces with a repulsive core [3–5,39–49] as well as effective interactions such as the Gogny force [48,50,51], provided that the BCS approximation (equivalent to the HFB in finite nuclei) is assumed. It is straightforward then to determine the wave function of the neutron Cooper pair from the solution of the gap equation [3,39,40,43–45,47,48]. This provides us

*Electronic address: matsuo@nt.sc.niigata-u.ac.jp

with a good reference frame to study the spatial structure of the Cooper pair as a function of the density, while I do not intend to make precise predictions of other properties of neutron and symmetric nuclear matter. I shall perform an analysis employing both a bare force and the effective Gogny force [52] and using a Hartree-Fock single-particle spectrum associated with the media. The main conclusion will be that the spatial dineutron correlation is strong in a wide range of low densities, $\rho/\rho_0 \approx 10^{-4} - 0.5$, independently of the adopted forces. I shall clarify the nature of the strong spatial dineutron correlation in terms of the BCS-BEC crossover model.

I shall also examine the possibility of phenomenological description of the spatially correlated neutron Cooper pair. Here I consider a contact force with a parametrized density-dependent interaction strength, often called the density-dependent δ interaction (DDDI) [8–11,53–58]. The parameters of the DDDI need to be determined from some physical constraints. For example, the interaction strength has been constrained by conditions intended to reproduce the experimentally extracted pairing gap in finite nuclei [9–11,54–57] or the density dependence of the neutron pairing gap in symmetric nuclear matter and the ^1S scattering length [8,58]. It should be noted here that the contact force requires a cutoff energy, which needs to be treated as an additional model parameter. Concerning the cutoff parameter, attention has been paid in previous studies to convergence properties of the pairing correlation energy in finite nuclei [9], to the energy dependence of the phase shift [59], or to renormalization with respect to the pairing gap [60,61]. In the present paper I shall take a different approach to the cutoff; i.e., I investigate the relevance of the cutoff parameter to the spatial structure of the neutron Cooper pair. It will be shown that the cutoff energy plays an important role in describing the strong spatial correlation at low density. Considering this a physical constraint on the cutoff energy, I shall derive new parameter sets for the DDDI.

Preliminary results of this work are reported in Ref. [62].

II. FORMULATION

A. BCS approximation

The neutron pair correlation in uniform neutron matter and in uniform symmetric nuclear matter is described by means of the BCS approximation, which is equivalent to Bogoliubov's generalized mean-field approach [26,27]. One of the basic equations is the gap equation, which is written in the momentum representation as

$$\Delta(p) = -\frac{1}{2(2\pi)^3}\int d\boldsymbol{k}\tilde{v}(\boldsymbol{p}-\boldsymbol{k})\frac{\Delta(k)}{E(k)}, \tag{1}$$

$$E(k) = \sqrt{[e(k)-\mu]^2 + \Delta(k)^2}. \tag{2}$$

Here $\Delta(k)$ is the pairing gap dependent on the single-particle momentum k, while $e(k)$ and $E(k)$ are the single-particle and the quasiparticle energies. $\tilde{v}(\boldsymbol{p}-\boldsymbol{k})$ is the matrix element of the nucleon-nucleon interaction in the ^1S channel. The gap equation needs to be solved together with the number equation

$$\rho \equiv \frac{k_F^3}{3\pi^2} = \frac{1}{(2\pi)^3}\int d\boldsymbol{k}\left[1 + \frac{e(k)-\mu}{E(k)}\right], \tag{3}$$

which determines the relation between the neutron density ρ (the Fermi momentum k_F) and the chemical potential μ. The solution of these equations defines the ground state wave function of the BCS type and the static pairing properties at zero temperature for a given density ρ.

As the interaction acting in the ^1S channel I shall adopt a bare nucleon-nucleon force, the G3RS force [63], and the effective interaction given by Gogny [52]. The G3RS force is a local potential representation of the bare nucleon-nucleon interaction, which is given by a superposition of three Gaussian functions:

$$v(\boldsymbol{r}) = \sum_i v_i e^{-r^2/\mu_i^2}. \tag{4}$$

One component represents a repulsive core with the height of $v_1 = 2000$ MeV and the range parameter $\mu_1 = 0.447$ fm, while two other Gaussians with $v_{2,3} = -240, -5$ MeV and $\mu_{2,3} = 0.942, 2.5$ fm represent the attraction dominant for $1 \lesssim r \lesssim 3$ fm (see Fig. 1). In spite of the simple three-Gaussian representation, the G3RS reproduces rather well the ^1S phase shift up to about 300 MeV in the c.m. energy of the scattering nucleons. The associated scattering length $a = -17.6$ fm is in close agreement with the experimental value $a = -18.5 \pm 0.4$ fm [64]. The G3RS has been used in some BCS calculations for the ^1S pairing at low density and for the $^3P_2$ pairing at high density [3–5]. From a practical point of view, the analytic form makes it easy to evaluate the matrix elements of the interaction.

The Gogny force is an effective interaction that is designed for the HFB description of the pairing correlation in finite nuclei while keeping some aspects of the G matrix [52]. It is also a local potential represented as a combination of two Gaussian functions in the form of Eq. (4) with the range parameters $\mu_{1,2} = 0.7, 1.2$ fm. In the following I present mostly results obtained with the parameter set D1 [52], as I find no qualitative difference in the results for the parameter set D1S [65]. A common feature of the G3RS and Gogny forces

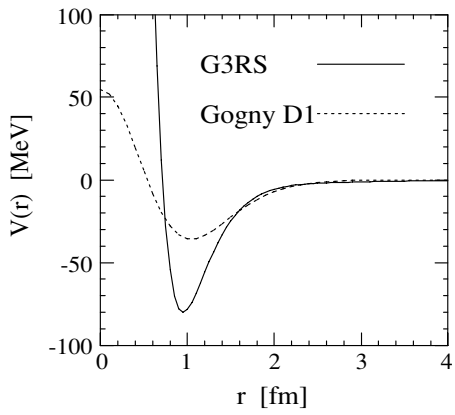

FIG. 1. Nucleon-nucleon potential $v(r)$ in the ^1S channel for the G3RS and Gogny D1 forces, plotted with the solid and dotted curves, respectively, as a function of the relative distance r between neutrons.

is that both are attractive in the range $1 \lesssim r \lesssim 3$ fm, while they differ largely for $r \lesssim 0.5$ fm, where the Gogny force exhibits only a very weak repulsion instead of the short-range core present in the G3RS force (Fig. 1). The interaction range of the two forces is of the order of 3 fm. Note that the experimental effective range is $r_e = 2.80 \pm 0.11$ [64]. I shall also apply a zero-range contact force $v(\boldsymbol{r}) \propto \delta(\boldsymbol{r})$. The treatment of this interaction will be described separately in Sec. V.

As the single-particle energy $e(k)$ I use, in the case of the Gogny interaction, the Hartree-Fock (HF) single-particle spectrum derived directly from the same interaction. In the case of the bare force, it would be better from the viewpoint of self-consistency to use the Brueckner Hartree-Fock spectrum. But for simplicity I adopt in the present analysis an effective mass approximation. Namely, the single-particle energy is given by $e(k) = k^2/2m^*$, where the effective mass $m^* = (\partial^2 e(k)/\partial^2 k|_{k_F})^{-1}$ is derived from the Gogny HF spectrum [50] for the parameter set D1.

The gap and number eqs. (1) and (3) are solved, without introducing any cutoff. The momentum integrations in the two equations are performed by using a direct numerical method, where the maximum momentum $k_{\max}$ for the integration is chosen large enough that the result does not depend on the choice of $k_{\max}$. I adopt $k_{\max} = 20$ fm^{-1} for the G3RS and $k_{\max} = 10$ fm^{-1} for the Gogny interaction. Note here that it is dangerous to introduce a small energy window around the chemical potential (or the Fermi energy) or a cutoff at a small momentum in evaluating the r.h.s. of the gap equation. Such an approximation may be justified only in the case of the weak coupling BCS, where the pairing gap is considerably smaller than the Fermi energy, but it is not applicable to the strong coupling case [30]. Note also that the chemical potential μ and the Fermi energy e_F are not the same except in the limit of weak coupling. I define the Fermi momentum k_F through the nominal relation to the density $\rho = (1/3\pi^2)k_F^3$, and the Fermi energy e_F as $e_F \equiv e(k_F)$. The pairing gap $\Delta_F \equiv \Delta(k_F)$ at the Fermi momentum is used below as a measure of the pair correlation. In the following ρ always denotes the neutron density. (The total nucleon density is $\rho_{\rm tot} = 2\rho$ in the case of symmetric nuclear matter.) I define, as a reference value, the normal neutron density as $\rho_0 = (1/3\pi^2)k_{F0}^3$ with $k_{F0} = 1.36$ fm^{-1}.

To investigate the spatial structure of the neutron Cooper pair, it is useful to look into its wave function represented as a function of the relative distance between the partner neutrons of the pair. It is given by

$$\Psi_{\rm pair}(r) \equiv C'\langle\Phi_0|\psi^\dagger(\boldsymbol{r}\uparrow)\psi^\dagger(\boldsymbol{r}'\downarrow)|\Phi_0\rangle = \frac{C}{(2\pi)^3}\int d\boldsymbol{k} u_k v_k e^{i\boldsymbol{k}\cdot(\boldsymbol{r}-\boldsymbol{r}')}, \quad (5)$$

$$u_k v_k = \frac{\Delta(k)}{2E(k)}, \quad (6)$$

in terms of the u, v factors except by the normalization factors C and C'. Here $\psi^\dagger(\boldsymbol{r}\sigma)$ ($\sigma = \uparrow, \downarrow$) is the creation operator of the neutron and $|\Phi_0\rangle$ is the BCS ground state. The Cooper pair wave function depends only on the relative distance $r = |\boldsymbol{r} - \boldsymbol{r}'|$ between the partners, as it is an s wave. I evaluate the momentum integral in Eq. (5) in the same way as in the gap and the number equations.

It is useful to evaluate the size of the neutron Cooper pair. A straightforward measure is the rms radius of the Cooper pair

$$\xi_{\rm rms} = \sqrt{\langle r^2\rangle}, \quad (7)$$

where

$$\langle r^2\rangle = \int d\boldsymbol{r} r^2 |\Psi_{\rm pair}(r)|^2 = \frac{\int_0^\infty dk k^2 \left(\frac{\partial}{\partial k} u_k v_k\right)^2}{\int_0^\infty dk k^2 (u_k v_k)^2} \quad (8)$$

can be calculated directly from the Cooper pair wave function $\Psi_{\rm pair}(r)$ and/or from the u, v factors in the momentum space. If one assumes weak coupling, Pippard's coherence length [32]

$$\xi_P = \frac{\hbar^2 k_F}{m^* \pi \Delta_F} \quad (9)$$

given analytically in terms of the gap and the Fermi momentum may also be used as another estimate of the size of the Cooper pair. In the following I mostly use $\xi_{\rm rms}$, since this quantity itself has a solid meaning even in the strong coupling BEC case and in the crossover region between BCS and BEC. I shall use ξ_P for qualitative discussions.

In the present paper, I neglect higher-order many-body effects that go beyond the BCS approximation. In many calculations [66–75] the higher-order effects in low-density neutron matter are predicted to reduce the pairing gap by about a factor of two, which is, however, very much dependent on the prescriptions adopted [4,5], except for the low-density limit $\rho \to 0$ [76]. A recent Monte Carlo study [77] using the realistic bare force suggests a gap close to the BCS result. The higher-order effects in symmetric nuclear matter [75] and in finite nuclei [78–80] are estimated to increase the gap. Keeping in mind these ambiguities, I consider that the BCS approximation provides a meaningful zeroth-order reference.

B. Pairing gap and coherence length

Figure 2 shows the neutron pairing gap Δ_F obtained with the G3RS and Gogny D1 forces both for neutron matter and for symmetric matter. Results assuming the free single-particle spectrum (equivalent to the use of $m^* = m$) are also shown for comparison. The pairing gap becomes maximum around $\rho/\rho_0 \sim 0.1-0.3$ in all the cases. The gap decreases gradually with further decreases in the density. The difference between neutron matter and symmetric nuclear matter, which originates from the effective mass effect, becomes negligible at low density $\rho/\rho_0 \lesssim 5 \times 10^{-2}$.

The pairing gap obtained with the G3RS force is very similar to those obtained with more realistic models of the bare force (OPEG [3,42,43], Reid [3,43,46], Argonne [44,46], Paris [44], Bonn [45,48], Nijmegen [4]). This is because the gap is essentially determined by the ^1S phase shift function [81], and the G3RS force reproduces the experimental phase shift, though not as accurately as the modern forces. There is small difference from them: the maximum gap $\Delta_F \approx 2.5$ MeV around $\rho/\rho_0 \sim 0.2$ (or $k_F \sim 0.8$ fm^{-1}) for neutron matter is slightly smaller in the G3RS by about 5%–20%. The difference may be due to a limitation of the simple three-

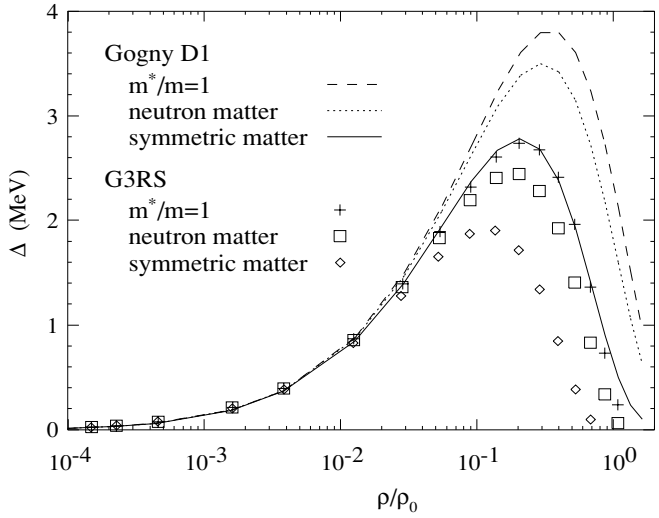

FIG. 2. Pairing gap Δ_F in neutron and symmetric nuclear matter as a function of the neutron density ρ/ρ_0. The results for the G3RS force are shown with the symbols: cross, free single-particle spectrum, square, neutron matter, diamond, symmetric matter. The results with the Gogny D1 force are plotted with the dashed, dotted, and solid curves for matter with the free single-particle spectrum, for neutron matter, and for symmetric matter, respectively.

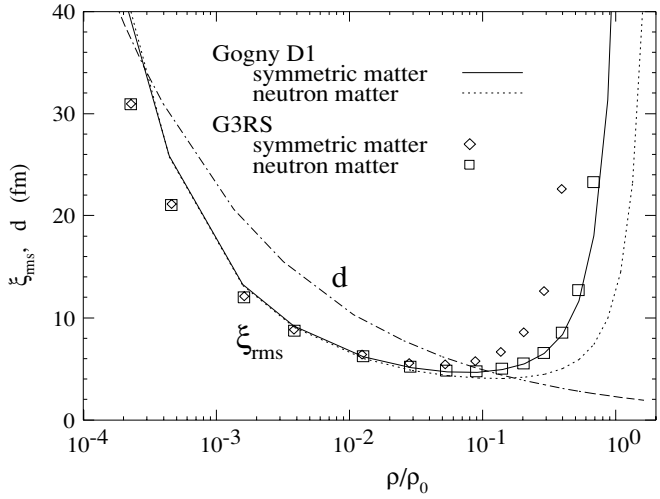

FIG. 3. The rms radius $\xi_{\rm rms}$ of the neutron Cooper pair in uniform matter, plotted as a function of the neutron density ρ/ρ_0. The results for symmetric nuclear and neutron matter obtained with the Gogny D1 force are shown by the solid and dotted curves, respectively, while the results for symmetric nuclear and neutron matter with the G3RS force are shown by the diamond and square symbols, respectively. The average interneutron distance $d = \rho^{-1/3}$ is plotted with the dotted-dashed curve.

Gaussian representation, but the quality is enough for the following discussions. The gap obtained with the Gogny force is consistent with those in the previous calculations [48,50,51]. If the Gogny and G3RS results are compared, they exhibit a similar overall density dependence, and a significant difference between the two forces is seen only at modest density $\rho/\rho_0 \gtrsim 5 \times 10^{-2}$. Garrido *et al.* [58] suggest that the similarity may indicate a possible cancellation among higher-order effects in the case of symmetric matter. A less significant difference in the gap is also found at rather low density $\rho/\rho_0 \lesssim 10^{-3}$, though it is not visible in Fig. 2. This arises from the fact that the scattering length $a = -13.5$ fm of the Gogny D1 force deviates from the G3RS value $a = -17.6$ fm.

The rms radius $\xi_{\rm rms}$ of the neutron Cooper pair calculated for neutron and symmetric nuclear matter with the bare or the Gogny forces is shown in Fig. 3 and Table I. The calculated $\xi_{\rm rms}$ is consistent with the rms radius (or Pippard's coherence length) reported in the BCS calculations by using other models of the bare force [3,43,47,48]. Here I emphasize the characteristic density dependence of $\xi_{\rm rms}$. It is seen from Fig. 3 that $\xi_{\rm rms}$ decreases dramatically, by nearly a factor of ten, from a large value of the order of $\sim$50 fm around the normal densities $\rho/\rho_0 \sim 1$ to considerably smaller values $\xi_{\rm rms} \approx 4.5$–$6$ fm at densities around $\rho/\rho_0 \sim 0.1$. The size of the Cooper pair stays at small values $\xi_{\rm rms} \approx 5$–6 fm in the density region $\rho/\rho_0 \sim 10^{-2} - 0.1$. It then turns to increase, but only gradually, at lower densities. These features are commonly seen for both neutron and symmetric nuclear matter and for both the G3RS and Gogny forces.

I emphasize also the smallness of the neutron Cooper pair. This may be elucidated if one compares the rms radius $\xi_{\rm rms}$ with the average interneutron distance $d \equiv \rho^{-1/3} = 3.09 k_F^{-1}$. It is seen from Fig. 3 that $\xi_{\rm rms}$ becomes smaller than d in a very wide range of densities $\rho/\rho_0 \sim 10^{-4} - 0.1$. The ratio $\xi_{\rm rms}/d$ can reach values as small as $\approx$0.5 at densities around $\rho/\rho_0 \sim 10^{-2}$. The relation $\xi_{\rm rms} < d$, i.e., a neutron Cooper pair smaller than the average interneutron distance, suggests that the neutron Cooper pair exhibits strong spatial dineutron correlation.

To understand this strong spatial correlation, it is useful to consider the ratio Δ_F/e_F between the pairing gap and the Fermi energy rather than the absolute magnitude of the gap. The pairing gap $\Delta_F \approx 0.2$ MeV at the density $\rho/\rho_0 = 1/512$, for example, appears small on the absolute scale, but the gap-to-Fermi-energy ratio amounts to $\Delta_F/e_F \approx 0.4$ (see Table I), which is larger than the value $\Delta_F/e_F \approx 0.25$ at $\rho/\rho_0 = 1/8$, where the gap is nearly maximum. If one uses Pippard's coherence length $\xi_P = \hbar^2 k_F/m^*\pi\Delta_F$ in place of the rms radius $\xi_{\rm rms}$ (this may be justified at least for qualitative discussion, since the two quantities agree within 10%–25%, see Table I), the ratio between the rms radius and the average interneutron distance is related to the gap-to-Fermi-energy ratio as $\xi_{\rm rms}/d \sim \xi_P/d \sim 0.2 e_F/\Delta_F$. Consequently, one can expect in the zeroth-order argument that the strong spatial correlation $\xi_{\rm rms}/d \lesssim 1$ emerges when the gap-to-Fermi-energy ratio is larger than $\Delta_F/e_F \gtrsim 0.2$. This is realized in the present calculations in the density range $\rho/\rho_0 \sim 10^{-4} - 0.1$. In the following I shall investigate in detail the spatial correlation in the neutron Cooper pair around this density range.

I comment here on a comparison with the $^3SD_1$ neutron-proton pairing in symmetric nuclear matter. In this case the BCS pairing gap calculated with a realistic bare force (the Paris force) is of the order of 8 MeV at maximum [49]. The rms radius $\xi_{\rm rms}$ of the neutron-proton Cooper pair is quite small, reaching the minimum value $\xi_{\rm rms} \sim 2$ fm at a density

TABLE I. Pairing gap Δ_F, rms radius $\xi_{\rm rms}$, Pippard's coherence length ξ_P, and probability $P(d)$ within the average interneutron distance d associated with the neutron Cooper pair in symmetric nuclear matter obtained with the Gogny D1 interaction and in neutron matter with the G3RS force, at the neutron density $\rho/\rho_0 = 1, 1/2, 1/8, 1/64, 1/512$ or, equivalently, $k_F = 1.36, 1.094, 0.68, 0.34, 0.17$ fm^{-1}. The Fermi energy e_F, the effective mass m^*/m, and the average interneutron distance d are also shown. The parameters $(1/k_F a)_\xi$ and $(1/k_F a)_\Delta$ of the regularized δ interaction model are also listed (see text). The units for k_F and Δ_F, e_F are fm^{-1} and MeV, respectively while that for d, $\xi_{\rm rms}$, and ξ_P is fm.

k_F	ρ/ρ_0	d	m^*/m	e_F	Δ_F	$\xi_{\rm rms}$	ξ_P	$P(d)$	$(1/k_F a)_\xi$	$(1/k_F a)_\Delta$
					Symmetric matter, Gogny D1					
1.36	1	2.27	0.668	62.0	0.64	46.60	41.76	0.18	−2.91	−2.99
1.079	1/2	2.87	0.744	33.8	2.03	10.80	9.45	0.48	−1.83	−1.84
0.68	1/8	4.55	0.891	10.9	2.60	4.81	3.87	0.81	−0.97	−0.90
0.34	1/64	9.10	0.984	2.45	0.97	5.87	4.71	0.92	−0.59	−0.52
0.17	1/512	18.20	0.998	0.60	0.22	12.05	10.30	0.91	−0.62	−0.58
					Neutron matter, G3RS					
1.36	1	2.27	0.905	42.4	0.14	159.8	144.1	0.09	−3.70	−3.70
1.079	1/2	2.87	0.925	26.1	1.52	11.61	10.13	0.47	−1.88	−1.85
0.68	1/8	4.55	0.969	9.89	2.37	4.94	3.90	0.80	−0.99	−0.90
0.34	1/64	9.10	0.995	2.41	0.98	5.90	4.61	0.92	−0.60	−0.50
0.17	1/512	18.20	0.999	0.60	0.24	11.16	9.30	0.92	−0.55	−0.50

around $\rho/\rho_0 \sim 0.2$ [40]. Consequently, the rms radius $\xi_{\rm rms}$ becomes considerably smaller than the average interparticle distance d in the density interval from $\rho/\rho_0 \sim 0.5$ down to the zero-density limit, where $\xi_{\rm rms}$ becomes identical to the rms radius of the deuteron [40]. In the case of the ^1S neutron pairing, by contrast, the signature of the strong coupling $\xi_{\rm rms} \lesssim d$ is obtained in the wide but limited range of the density $\rho/\rho_0 \sim 10^{-4} - 0.1$. Apart from this difference, it is noted that the qualitative trend of the Cooper pair size, e.g., size shrinking from the zero-density limit, is similar to that discussed in the neutron-proton case [40].

III. SPATIAL STRUCTURE OF NEUTRON COOPER PAIR

A. Cooper pair wave function: basics

In examining the spatial structure of the neutron Cooper pairs, I shall focus mostly on the symmetric nuclear matter case obtained with the Gogny force and the neutron matter case with the G3RS force. The rms radii in these two cases represent a rough mean value of the four results plotted in Fig. 3. Note also that the two rms radii coincide with each other within 10% over a very wide interval of densities $\rho/\rho_0 = 10^{-3} - 0.5$. It is by accident, but this feature can be exploited to single out influences of different interactions, since the comparison can be made with the rms radii kept the same.

Figures 4(a)–4(e) show the wave function $\Psi_{\rm pair}(r)$ of the neutron Cooper pair for the representative values of density listed in Table I. The result for neutron matter calculated with the G3RS force and that for symmetric nuclear matter with the Gogny D1 force are plotted in the same figure for the reasons mentioned just above. The probability density $r^2|\Psi_{\rm pair}(r)|^2$ multiplied by the volume element r^2 is plotted in Figs. 4(f)–4(j).

As a quantitative measure of the spatial correlation, I also evaluate the probability $P(r)$ for the partners of the neutron Cooper pair to come close to each other within a relative distance r, which is nothing but a partial integration of the probability density $r^2|\Psi_{\rm pair}(r)|^2$ up to the distance r:

$$P(r) = \frac{\int_0^r |\Psi_{\rm pair}(r')|^2 r'^2 dr'}{\int_0^\infty |\Psi_{\rm pair}(r')|^2 r'^2 dr'}. \tag{10}$$

An example of this quantity is shown in Fig. 5 for the case $\rho/\rho_0 = 1/2$.

Before proceeding to the main analysis, I first point out that the G3RS and Gogny forces provide essentially the same spatial structure of the Cooper pair except at very short relative distances. In Fig. 4 a clear difference between the two forces is seen at short relative distances $r \lesssim 1$ fm. (Note that the normal density case, Figs. 4(a) and 4(f), is not relevant for this discussion, since the gaps and the rms radii are very different.) Apparently the suppression of the wave function seen at $r \lesssim 1$ fm in the G3RS case is caused by the strong repulsive core present in the bare force. The Cooper pair wave function for the Gogny force does not show this short-range correlation because of the lack of the core. On the other hand, by looking at distances $r > 1$ fm, slightly larger than the core radius, one finds that the Cooper pair wave functions obtained with the two forces agree quite well with each other. This observation also applies to the probability density $r^2|\Psi_{\rm pair}(r)|^2$ and the probability $P(r)$, for which the difference at short distances $r < 1$ fm becomes barely visible, as the volume element is small at such short distances. Thus the spatial structure of the neutron Cooper pair does not depend on whether the interaction is the bare force or the effective Gogny force, provided that two cases gives the same rms radius of the Cooper pair. In the following, I shall concentrate on behaviors that are common to the two interactions.

The Cooper pair wave function $\Psi_{\rm pair}(r)$ in the coordinate representation is reported in some of the previous BCS calculations adopting other models of the bare force [43–45,47,48] and the Gogny force [48]. The wave function appears consistent with those in Refs. [43–45,48], although

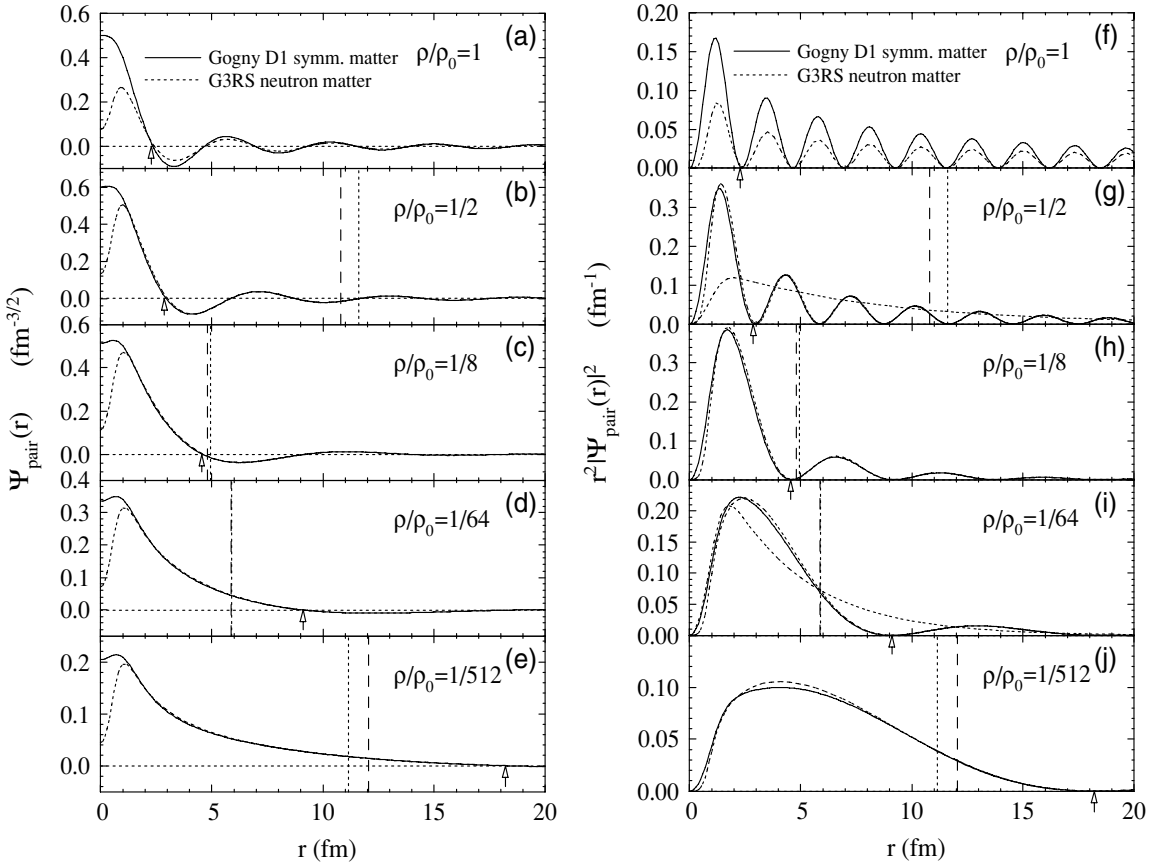

FIG. 4. (a)–(e) Wave function $\Psi_{\rm pair}(r)$ of the neutron Cooper pair as a function of the relative distance r between the pair partners at the neutron density $\rho/\rho_0 = 1, 1/2, 1/8, 1/64, 1/512$. The solid curve is for the pair in symmetric nuclear matter obtained with the Gogny D1 force, while the dotted curve is for that in neutron matter with the G3RS. The vertical dotted line represents the rms radius $\xi_{\rm rms}$ of the Cooper pair in neutron matter with the G3RS, while the dashed line is for symmetric nuclear matter with Gogny D1. Here and also in the following figures the wave function is normalized by $\int_0^\infty |\Psi_{\rm pair}(r)|^2 r^2 dr = 1$. The arrow indicates the average interneutron distance d. (f)–(j) The same as (a)–(e) but for the probability density $r^2|\Psi_{\rm pair}(r)|^2$. The thin dotted curve in (g) and (i) is the wave function of the fictitious bound state in the free space described in the text.

in these references the wave function is shown only at very limited numbers of density values and not up to very large relative distances. I found, however, that the shape of the Cooper pair wave function shown in Ref. [47] differs markedly from the present results (Fig. 4), especially at relative distances smaller than several femtometers.

B. Density dependence

If the Cooper pair wave functions at different density values are compared in Fig. 4, important features show up. An apparent observation is that the spatial extension or the size of the Cooper pair varies strongly with the density, in accordance with the strong density dependence of the rms radius $\xi_{\rm rms}$ discussed in the previous section (Fig. 3). I emphasize here another prominent feature, namely, that *profile* of the Cooper pair wave function also changes significantly with the density.

At normal density, $\rho/\rho_0 = 1$ [Figs. 4(a) and 4(f)], the Cooper pair wave function is spatially extended: the rms radius of the Cooper pair is as large as $\xi_{\rm rms} \gtrsim 50$ fm. The profile of the Cooper pair wave function in this case exhibits an exponential falloff convoluted with an oscillation. This behavior is consistent with the well-known expression [32] $r\Psi_{\rm pair}(r) \sim K_0(r/\pi\xi_P)\sin(k_F r)$ for the Cooper pair wave function in the weak coupling BCS situation. Here K_0 is the modified Bessel function, which behaves asymptotically as $K_0(r/\pi\xi_P) \sim (\xi_P/r)^{1/2}\exp[-(r/\pi\xi_P)]$. The position of the first node $r \approx \pi k_F^{-1}$ approximately corresponds to the average interparticle distance $d = 3.09k_F^{-1} (= 2.3$ fm). The wave function has significant amplitude for $r > d$, since here $\xi_{\rm rms,P} \gg d$ (see Table I). This is a typical behavior in the situation of the weak coupling BCS.

The Cooper pair wave function at the density $\rho/\rho_0 = 1/8$ [Figs. 4(c) and 4(h)] is very different from that at the normal density. Apart from the considerably small spatial extension ($\xi_{\rm rms} = 4.8-4.9$ fm), the functional form of the wave function behaves quite differently. It is found that the amplitude of the wave function is strongly concentrated within the average interneutron distance d and that the oscillating amplitude beyond d is quite small. This is consistent with the observation in the previous section that the rms radius $\xi_{\rm rms}$ of the Cooper

pair is smaller than the average interneutron distance d in this case (cf. Fig. 3 and Table I). The probability $P(d)$ for the partners of the Cooper pair to be correlated within the internucleon distance d exceeds 0.8 (Fig. 6 and Table I), indicating directly the strong spatial dineutron correlation.

The neutron Cooper pair wave functions at $\rho/\rho_0 = 1/64$ and 1/512 [Figs. 4(d), 4(e), 4(i), and 4(j)] exhibit a behavior similar to that at $\rho/\rho_0 = 1/8$. Inspecting more closely, one notices that the concentration within $r < d$ is stronger than at $\rho/\rho_0 = 1/8$, while the spatial extension itself is slightly larger ($\xi_{\rm rms} \approx 6-12$ fm). One also observes a smaller oscillating amplitude in the long-distance region $r > d$ (Fig. 4), larger values of $P(d) \approx 0.9$, and smaller ratio $\xi_{\rm rms}/d$ (Table I). They all point to stronger spatial dineutron correlation at these values of density.

The Cooper pair wave function at $\rho/\rho_0 = 1/2$ [Figs. 4(b) and 4(g)] exhibits an intermediate feature between that at the normal density $\rho/\rho_0 = 1$ and those at $\rho/\rho_0 = 1/64-1/512$. In particular, notice that the spatial correlation seen at the lower density also persists to some significant extent in this case. For example, the probability density is strongly concentrated to the short-distance region of $r \lesssim 3$ fm [Fig. 4(g)]. This is more apparent in the plot of $P(r)$, shown in Fig. 5, where one finds that the probability $P(r)$ increases steeply as r increases from $r = 0$ and already reaches ∼50% at $r = 3$ fm, which is roughly the interaction range of the nucleon force. This strong concentration within $r < 3$ fm may be elucidated by comparing with what could be expected if a bound pair having the same rms radius ($\xi_{\rm rms} = 10.8$ fm in this case) were formed in the free space. (I calculate this fictitious "bound state" wave function by increasing the strength of the Gogny D1 potential by a numerical factor.) It is noticed that the profile of the Cooper pair wave function differs from the "bound state" wave function which is plotted with the thin dotted curve in Fig. 4(g). In this "bound state" wave function, the concentration of the probability within $r \lesssim 3$ fm is not very large, i.e., $P(3\ {\rm fm}) = 0.24$, while the probability $P(3$ fm) associated

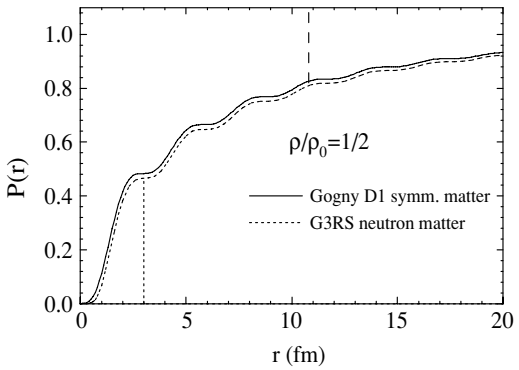

FIG. 5. Probability $P(r)$ for the partner neutrons of the Cooper pair to be correlated within a relative distance r, calculated at density $\rho/\rho_0 = 1/2$. The result for symmetric nuclear matter with the Gogny D1 force is plotted with the solid curve, while the dotted curve represents the result for neutron matter with the G3RS force. The dashed vertical line indicates the rms radius of the Cooper pair in the symmetric matter case. The vertical dotted line marks the position $r = 3$ fm.

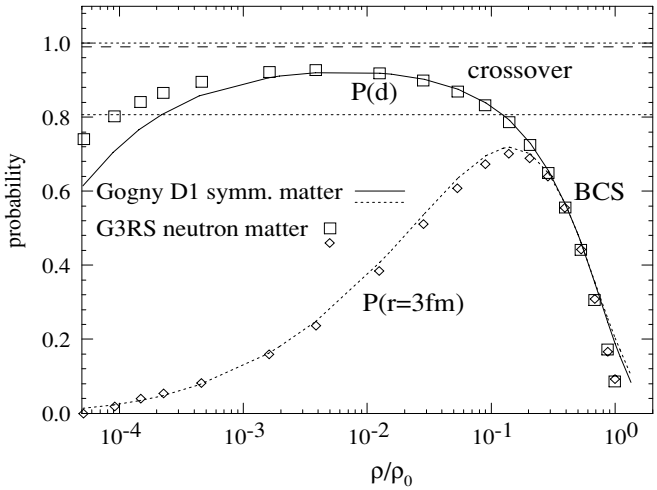

FIG. 6. Probability $P(d)$ for the partner neutrons to be correlated within the average interneutron distance d and the probability $P(3$ fm) within $r = 3$ fm. The solid and dotted curves are for symmetric nuclear matter obtained with the Gogny D1 force, while the square and diamond symbols are for neutron matter with the G3RS force.

with the neutron Cooper pair wave function is about twice this value. This indicates that the spatial dineutron correlation is also strong for the moderate low-density region $\rho/\rho_0 \sim 0.5$. A remnant of this spatial correlation is also found at the normal density [Figs. 4(a) and 4(f)], but in this case the concentration within the interaction range is not very large [$P(3\ {\rm fm}) = 0.21$], owing to the very large Cooper pair size ($\xi_{\rm rms} \sim 50$ fm). In contrast, the Cooper pair wave function at the lower density, $\rho/\rho_0 = 1/64$ [Fig. 4(i)], for example, is much more similar to the bound state wave function.

Figure 6 shows the overall behavior of $P(3$ fm) and $P(d)$ as a function of the density. It is seen that the strong concentration within the interaction range, say $P(3\ {\rm fm}) > 0.5$, is realized in the density region $\rho/\rho_0 \approx 5 \times 10^{-2}-0.5$. The probability $P(3$ fm) reaches the maximum value ∼0.7 around $\rho/\rho_0 \sim 0.1$, where the rms radius is the smallest. At lower density, $\rho/\rho_0 \lesssim 10^{-1}$, the probability $P(3$ fm) decreases gradually in accordance with the gradual increase of the rms radius of the Cooper pair. Note, however, that in this density region ($\rho/\rho_0 \sim 10^{-4}-10^{-1}$) the concentration of the probability within the average interneutron distance d remains very large, i.e., $P(d) \gtrsim 0.8$.

All the above analyses indicate that the spatial dineutron correlation is strong in the quite wide density interval $\rho/\rho_0 \sim 10^{-4}-0.5$.

It is interesting to compare the present result with that in a similar analysis of the Cooper pair wave function for the $^3SD_1$ neutron-proton pairing. In that case the Cooper pair wave function is found to merge smoothly into the deuteron wave function in the low-density limit [39]. Correspondingly, the rms radius of the Cooper pair approaches that of the deuteron, which is much smaller than the average interparticle distance [40]. This is interpreted as a realization of the BEC of the deuterons in the low-density region and the BCS-BEC crossover taking place with the change in the density [38–41]. In the neutron pairing case, the similarity of the Cooper pair

wave function to a bound state wave function is found only in a limited density range $\rho/\rho_0 \sim 10^{-4}-10^{-1}$, and it never converges to a bound state wave function (NB.: there is no bound state in this channel in the free space). The rms radius $\xi_{\rm rms}$ of the Cooper pair is only comparable with the average interneutron distance d in the same density interval. Although the spatial correlation is strong, as discussed above, these qualitative observations alone are not enough to assess whether the region of the BCS-BEC crossover is reached in the case of neutron pairing. I shall investigate this issue on a more quantitative bases in the next section.

IV. RELATION TO THE BCS-BEC CROSSOVER

In the previous section, I have shown the strong spatial correlation in the neutron Cooper pair wave function at low density. In the present section I shall elucidate its implication by making a connection to the BCS-BEC crossover phenomenon.

For this purpose, I shall first describe a reference Cooper pair wave function based on a simple solvable model of the BCS-BEC crossover and then compare the results with that of the reference model. As such a reference, I adopt a ^1S pairing model that applies generically to a dilute gas limit of any Fermion system [30,33,34], for which the average interparticle distance $d = \rho^{1/3}$ is supposed to be much larger than the range of interaction. The dilute limit is equivalent to treating the interaction matrix elements as a constant, or assuming a contact interaction. Using the relation between the interaction constant and the zero-energy T matrix or the scattering length a, the gap equation (1) is written in a regularized form:

$$\frac{m}{4\pi\hbar^2 a} = -\frac{1}{2(2\pi)^3}\int d\boldsymbol{k}\left[\frac{1}{E(k)} - \frac{1}{e(k)}\right]. \qquad (11)$$

The regularized gap equation (11) and the number equation (3) are now expressed analytically in terms of some special functions and are easily solvable [82,83]. In this model a dimensionless parameter $1/k_F a$, characterized by the scattering length and the Fermi momentum, is the only parameter that controls the strength of interaction, and hence properties of the pair correlation are determined solely by $1/k_F a$, while the length scale is given by k_F^{-1} (or the interparticle distance $d = 3.09k_F^{-1}$), and the energy scale by the Fermi energy $e_F = \hbar^2 k_F^2/2m$ [30,33–35,82]. The gap-to-Fermi-energy ratio Δ/e_F and the ratio $\xi_{\rm rms}/d$ between the rms radius and the average interparticle distance are then monotonic functions of the interaction parameter $1/k_F a$ [34,82]. The functional form of the Cooper pair wave function, defined by Eq. (5), is also determined only by $1/k_F a$, except for the length scale. Since there is no available analytic expression for the wave function, I evaluate Eq. (5) by performing the momentum integral numerically with a help of an explicit use of a smooth cutoff function of Gaussian form. The cutoff scale is chosen to be large enough that the results shown below do not depend on it.

The range $1/k_F a \ll -1$ of the interaction parameter corresponds to the situation of the weak coupling BCS, for which the pairing gap is given by the well-known formula [4,30,35] $\Delta/e_F \approx 8e^{-2}\exp(\pi/2k_F a)$. In the opposite range, $1/k_F a \gg 1$, the situation of Bose-Einstein condensation (BEC) of bound Fermion pairs (bosons) is realized. The crossover between the weak coupling BCS and the strong coupling BEC corresponds to the interval $-1 \lesssim 1/k_F a \lesssim 1$, as described in Refs. [30,33–35]. (The case with the infinite scattering length $1/k_F a = 0$ is the midpoint of the crossover, called the unitarity limit.) In the following I shall adopt $1/k_F a = \pm 1$ according to Ref. [34] as the boundaries characterizing the crossover, although the transition is smooth in nature.

TABLE II. Reference values of $1/k_F a$, $\xi_{\rm rms}/d$, and Δ/e_F characterizing the BCS-BEC crossover in the regularized δ interaction model.

$1/k_F a$	$\xi_{\rm rms}/d$	Δ/e_F	$P(d)$	
-1	1.10	0.21	0.807	boundary to BCS
0	0.36	0.69	0.990	unitarity limit
1	0.19	1.33	1.000	boundary to BEC

In Table II are listed the values of $\xi_{\rm rms}/d$ and Δ_F/e_F at the boundaries $1/k_F a = \pm 1$ of the crossover domain and at the unitarity limit $1/k_F a = 0$ [34,82]. Note that the rms radius comparable with the average interparticle distance $0.2 \lesssim \xi_{\rm rms}/d \lesssim 1.1$, or the gap comparable with the Fermi energy $0.2 \lesssim \Delta_F/e_F \lesssim 1.3$, corresponds to the BCS-BEC crossover domain $-1 \lesssim 1/k_F a \lesssim 1$. I have discussed in the previous section the probability $P(d)$ for the paired neutrons to come closer than the average interneutron distance d (cf. Fig. 6). As the same quantity is also easily calculated in the analytic model of the BCS-BEC crossover (the result is shown in Fig. 7), this quantity may also be used as a measure of the crossover. The calculated boundary values corresponding to $1/k_F a = \pm 1, 0$ are listed in Table II. The crossover region is specified by

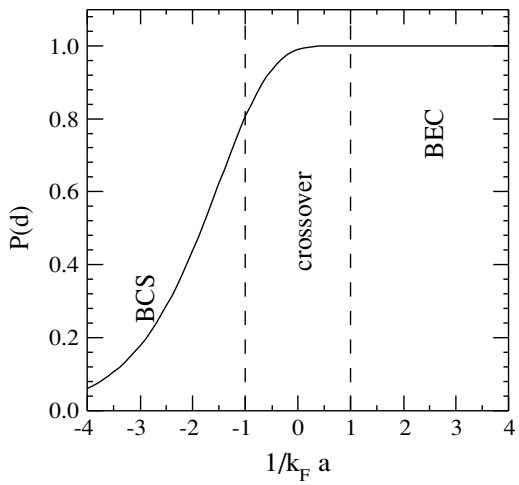

FIG. 7. Probability $P(d)$ for the partner particles to be correlated within the average interparticle distance d for the regularized δ interaction model.

$0.8 \lesssim P(d) \lesssim 1.0$, while the boundary to the strong coupling BEC regime [$P(d) \approx 1$] is hardly visible in this measure.

In the case of nucleonic matter, the assumption of the dilute gas limit may be justified only at very low density $\rho/\rho_0 \lesssim 10^{-5}$ (or $k_F \lesssim 0.05$ fm^{-1}) [4,46,84], and hence one cannot apply the above analytic model in a direct manner to the region of the density $\rho/\rho_0 = 10^{-5}-1$ which I am dealing with. In order to make the application possible, I adopt a more flexible viewpoint by regarding the interaction parameter $1/k_F a$ as a freely adjustable variable, rather than by fixing it from the physical value of the neutron scattering length. I shall call the model treated in this way the regularized δ interaction model to distinguish from the original idea of the dilute gas limit.

The interaction parameter $1/k_F a$ needs to be determined, then. I shall require the condition that the regularized δ interaction model give, for a given value of density, the same rms radius $\xi_{\rm rms}/d$ as that of the microscopically calculated neutron Cooper pair. The parameter determined in this way may be denoted $(1/k_F a)_\xi$. One can also determine the interaction parameter to reproduce the ratio Δ_F/e_F between the gap and the Fermi energy, which I shall denote $(1/k_F a)_\Delta$. The values of $(1/k_F a)_\xi$ and $(1/k_F a)_\Delta$ thus determined are listed in Table I. There is no sizable difference between $(1/k_F a)_\xi$ and $(1/k_F a)_\Delta$. The Cooper pair wave functions obtained in this reference model are shown in Fig. 8. It is hard to distinguish between the two options of $1/k_F a$. Let us compare them with the neutron Cooper pair wave function obtained with the Gogny force for symmetric matter at the three representative values of density $\rho/\rho_0 = 1$, 1/8, and 1/512.

It is seen from Fig. 8 that the wave function of the regularized δ interaction model and and that of the neutron Cooper pair behave very similarly at distances far outside the interaction range, $r \gtrsim 5$ fm. In contrast, there is a sizable disagreement for $r \lesssim 3$ fm. The disagreement is understandable, as the wave function within the interaction range $r \approx 3$ fm of the finite range Gogny force could not be described by the zero-range δ interaction. The Cooper pair wave function in the regularized δ interaction model exhibits the known divergence $\Psi_{\rm pair}(r) \propto 1/r$ for $r \to 0$ [cf. Figs. 8(a)–8(c)], and consequently the disagreement between the Gogny model and the regularized δ interaction model becomes serious at very short relative distances $r \lesssim 1$ fm. Note, however, that the squared wave function weighted with the volume element r^2 stays finite as seen in Figs. 8(d)–8(f) and hence there is no diverging difference in the probability density. These observations suggest that the regularized δ interaction model can account for the essential features of the spatial structure of the neutron Cooper pair if the interaction strength $1/k_F a$ is chosen appropriately.

We thus have a reference frame, i.e., the regularized δ interaction model, to which the neutron pairing is mapped. The question of the possible relation to the BCS-BEC crossover phenomena can be addressed now quantitatively. Let us first look into the ratio $\xi_{\rm rms}/d$ between the rms radius $\xi_{\rm rms}$ of the Cooper pair and the average interparticle distance d. The values of $\xi_{\rm rms}/d$ for the neutron Cooper pair obtained with the G3RS force and the Gogny D1 interaction are compared in Fig. 9 with the reference values defining the boundaries of the BCS-BEC crossover domain (Table II). It is seen in Fig. 9 that the calculated ratio $\xi_{\rm rms}/d$ enters the domain of the BCS-BEC crossover, $1.10 > \xi_{\rm rms}/d (> 0.19)$, in the density interval $\rho/\rho_0 \approx 10^{-4}-0.1$. Note also that calculated ratio becomes closest to the unitarity limit $\xi_{\rm rms}/d = 0.36$ around the density $\rho/\rho_0 \sim 10^{-2}$. From another point of view, the weak coupling BCS regime is realized only at very low density, $\rho/\rho_0 \lesssim 10^{-4}$, and around the normal density, $\rho/\rho_0 \gtrsim 0.2$.

Comparing in Fig. 10 the gap-to-Fermi-energy ratio Δ_F/e_F with the boundary values $0.21 < \Delta_F/e_F < 1.33$ leads to the same observation, that the density region $\rho/\rho_0 \sim 10^{-4}-0.1$ corresponds to the domain of the BCS-BEC crossover. Comparison of the third measure $P(d)$, shown in Fig. 6, provides

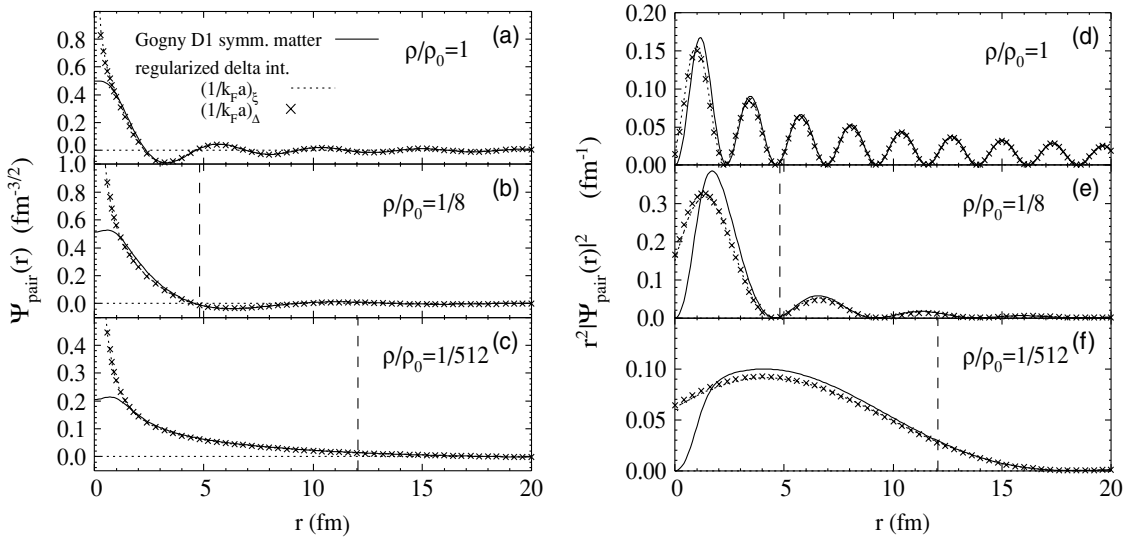

FIG. 8. (a)–(c) Neutron Cooper pair wave function $\Psi_{\rm pair}(r)$ in the regularized δ interaction model, plotted with the dotted curve and the cross symbols in the cases of $(1/k_F a)_\xi$ and $(1/k_F a)_\Delta$, respectively. The neutron Cooper pair wave function in symmetric nuclear matter obtained with the Gogny D1 force is also shown by the solid curve. (d)–(f) The same as (a)–(c) but for the probability density $r^2|\Psi_{\rm pair}(r)|^2$.

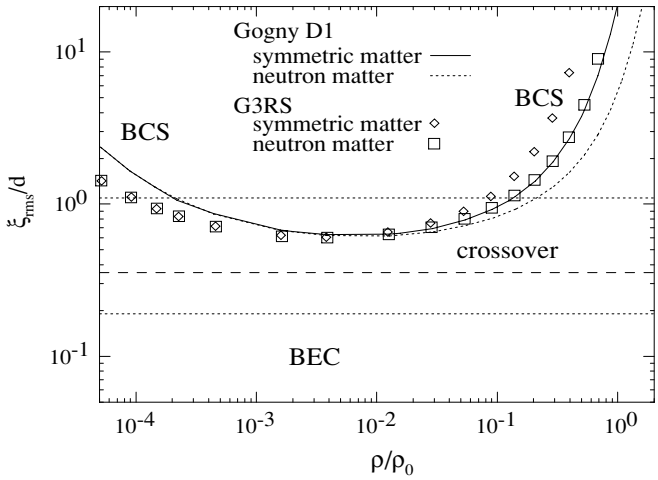

FIG. 9. Ratio $\xi_{\rm rms}/d$ between the rms radius $\xi_{\rm rms}$ of the neutron Cooper pair and the average internucleon distance d, calculated with the Gogny D1 force for symmetric nuclear and neutron matter (the solid and dotted curves, respectively), and those with the G3RS force for symmetric nuclear and neutron matter (the diamond and square symbols), plotted as a function of the neutron density. The reference values characterizing the BCS-BEC crossover listed in Table II are also shown as the horizontal dotted and dashed lines.

us the same information. It is also seen in the values of $(1/k_F a)_\xi$ and $(1/k_F a)_\Delta$ listed in Table I that the condition of the crossover region $(1/k_F a)_{\xi,\Delta} > -1$ is met in the cases $\rho/\rho = 1/8, 1/64, 1/512$.

On the basis of the above analysis, it is concluded that the strong spatial correlation at short relative distances seen in the neutron Cooper pair in the very wide density range $\rho/\rho_0 \approx 10^{-4}$–$0.1$ is the behavior associated with the BCS-BEC crossover.

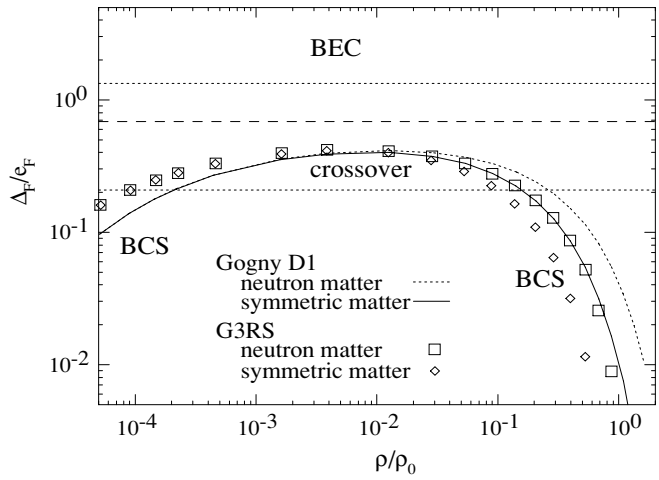

FIG. 10. Ratio Δ_F/e_F between the neutron pairing gap Δ_F and the neutron Fermi energy e_F, plotted as a function of the neutron density. The curves and the symbol are the same as in Fig. 9. The reference values characterizing the BCS-BEC crossover listed in Table II are also shown as the horizontal lines.

V. DENSITY-DEPENDENT δ INTERACTION

A. DDDI and the cutoff energy

The contact force whose interaction strength is chosen as a density-dependent parameter, often called the density-dependent δ interaction (DDDI), has been employed as a phenomenological effective interaction describing the pairing correlation in finite nuclei, especially unstable nuclei with large neutron excess [9–11,25,61,85–88]. In the previous section I showed that the regularized contact interaction model, which also employs the contact force but with an analytic regularization, describes the essential feature of the spatial structure of the neutron Cooper pair wave function over the whole density range. This suggests the possibility that the phenomenological DDDI may describe the spatial correlation in the neutron pairing. I would like to examine from this viewpoint under what conditions the DDDI can be justified.

The density-dependent δ interaction has a form

$$v(\boldsymbol{r}) = \frac{1-P_\sigma}{2} V_0[\rho]\delta(\boldsymbol{r}), \tag{12}$$

where $V_0[\rho]$ is the interaction strength that is supposed to be dependent on the density. The force acts only in the ^1S channel owing to the projection operator $(1-P_\sigma)/2$. It should be noted that in applications of the density-dependent δ interaction to finite nuclei an explicit and finite cutoff energy needs to be introduced. The cutoff energy in this case is regarded as an additional model parameter.

Applying the DDDI to the neutron pairing in uniform matter, the gap equation reads as

$$\Delta = -\frac{V_0}{2(2\pi)^3}\int' d\boldsymbol{k}\frac{\Delta}{E(k)}, \tag{13}$$

where the pairing gap is a momentum independent constant Δ. For the single-particle energy $e(k)$, the effective mass approximation is adopted, and the effective mass derived from the Hartree-Fock spectrum of the Gogny D1 is used. The momentum integral in Eq. (13) is performed under a sharp cutoff condition,

$$e(k) < \mu + e_{\rm cut}, \tag{14}$$

where the cutoff energy $e_{\rm cut}$ is defined as the relative energy from the chemical potential μ. I shall treat $e_{\rm cut}$ as a common constant that is applied to all densities. The same cutoff is used in calculating the Cooper pair wave function.

The present definition of the cutoff is different from a similar one adopted in Refs. [8,58], where a cutoff energy is defined with respect to the single-particle energy $e(k)$ measured from the bottom of the spectrum $e(k=0)$, e.g., by imposing $e(k) < 60$ MeV [58] independent of the density. In the present work, by contrast, an energy window above the chemical potential μ is fixed to $e_{\rm cut}$. I think that the cutoff energy $e_{\rm cut}$ defined in this way can be compared with the quasiparticle energy cutoff $E_i < E_{\rm cut}$ adopted often in the HFB calculations for finite nuclei (E_i is the quasiparticle energy of the single-particle state i) [9–11,25,28,61,85–88]. Note that in finite nuclei the density varies locally with the position coordinate, while the quasiparticle energy is defined globally. This may imply, in the sense of the local density approximation, that

TABLE III. The rms radius $\xi_{\rm rms}$ of the neutron Cooper pair in symmetric nuclear matter obtained with the density-dependent δ interaction and different cutoff energies $e_{\rm cut} = 5, 10, 30, 50, 100, 200$ MeV. In the rightmost column, the rms radius for the Gogny D1 force is also listed. The underline denotes that the calculated number agrees with the reference Gogny D1 result within 10%.

ρ/ρ_0	$\xi_{\rm rms}$ [fm]						
	$e_{\rm cut} = 5$	10	30	50	100	200 MeV	Gogny D1
1	48.6	47.3	46.7	46.6	46.5	46.5	46.6
1/2	16.9	13.8	11.2	10.9	10.7	10.6	10.8
1/8	14.9	10.0	6.0	5.3	4.8	4.6	4.8
1/64	10.5	7.9	6.2	6.0	5.7	5.5	5.9
1/512	13.2	12.5	12.0	11.9	11.8	11.7	12.1

a fixed density-independent cutoff quasiparticle energy $E_{\rm cut}$ is applied to each value of local density. Note also that both our $e_{\rm cut}$ and the cutoff quasiparticle energy $E_{\rm cut}$ are quantities measured from the chemical potential, which approximately coincide if $e_{\rm cut}$ and $E_{\rm cut}$ are sufficiently larger than the pairing gap. Thus one can compare directly $e_{\rm cut}$ and $E_{\rm cut}$, provided that $e_{\rm cut}$ is chosen as a density-independent constant. At the zero-density limit with $\mu = 0$, the cutoff energy $e_{\rm cut}$ simply defines an upper bound on the free single-particle energy $e(k) = \hbar^2 k^2/2m$.

B. Constraints on $e_{\rm cut}$

Let us investigate how the energy cutoff influences the Cooper pair wave function. I performed several calculations, using different values of $e_{\rm cut} = 5, 10, 30, 50, 100, 200$ MeV for symmetric nuclear matter. The value of the interaction strength V_0 is chosen for each value of the density so that the gap Δ calculated with a given cutoff energy $e_{\rm cut}$ coincides with the gap Δ_F obtained with the Gogny D1 force. Note that the interaction strength V_0 thus determined depends on both the cutoff energy and the density.

Table III shows the rms radius $\xi_{\rm rms}$ of the neutron Cooper pair calculated with the DDDI for different values of the cutoff energy. Here $\xi_{\rm rms}$ is calculated by using the Cooper pair wave function in the coordinate representation evaluated up to $r = 500$ fm. It is seen from Table III that the result apparently depends on the cutoff energy $e_{\rm cut}$. In the cases $\rho/\rho_0 = 1/64-1/2$, the dependence of $\xi_{\rm rms}$ on $e_{\rm cut}$ is very strong. The values calculated with the small cutoff energy $e_{\rm cut} = 5, 10$ MeV deviate greatly from those obtained with the Gogny force even though the interaction strength is chosen to reproduce the same reference pairing gap. It is concluded that the small cutoff energies $e_{\rm cut} = 5, 10$ MeV are unacceptable, since they fail to describe the small size $\xi_{\rm rms} \sim 5$ fm of the neutron Cooper pair at the density around $\rho/\rho_0 = 10^{-2}-0.1$. If one requires the DDDI to reproduce the rms radius of the neutron Cooper pair within an accuracy of 10% over the whole density region of interest, the use of a large value of the cutoff energy satisfying $e_{\rm cut} \gtrsim 50$ MeV is suggested.

To see the roles of the cutoff energy in more details, I show in Fig. 11 the neutron Cooper pair wave functions $\Psi_{\rm pair}(r)$ obtained for $e_{\rm cut} = 5, 10, 30, 50, 100$ MeV. The plot of $\Psi_{\rm pair}(r)$ clearly indicates that the Cooper pair wave function depends sensitively on the cutoff energy $e_{\rm cut}$. If one adopts the small cutoff energies $e_{\rm cut} = 5, 10$ MeV, the wave function obtained with the DDDI fails to produce the strong spatial correlation at the short relative distances $r \lesssim 3$ fm, which is the characteristic feature of the neutron Cooper pair wave function common to the Gogny and G3RS forces. (Figure 11 shows only the Gogny result for comparison, but the reader should be reminded of Fig. 4, where the G3RS case is also shown.) The plot of the probability density $r^2|\Psi_{\rm pair}(r)|^2$ at the density $\rho/\rho_0 = 1/8$ indicates that even the wave function at larger distances is not described well if the small cutoff energies $e_{\rm cut} = 5, 10$ MeV are adopted. This is nothing but the difficulty mentioned above in describing the rms radius with these small cutoff energies. If one uses a large cutoff energy, say, $e_{\rm cut} \gtrsim 30-50$ MeV, the wave function at large distances converges reasonably to that obtained with the Gogny force. Concerning the wave function at short relative distances $r \lesssim 3$ fm, on the other hand, no convergence is seen with respect to the cutoff energy. The value of the wave function $\Psi_{\rm pair}(0)$ at zero relative distance $r = 0$ increases monotonically with increasing $e_{\rm cut}$. (Increasing further, $e_{\rm cut} \to \infty$, $\Psi_{\rm pair}(r)$ will approach that for the regularized δ interaction model shown in Fig. 8, and the value $\Psi_{\rm pair}(0)$ at $r = 0$ will diverge.)

It may be possible to regard $e_{\rm cut}$ as a parameter that simulates the finite range of the neutron-neutron interaction. It is then reasonable to require that the wave function $\Psi_{\rm pair}(r)$ of the DDDI model with an appropriate choice of $e_{\rm cut}$ describe that of the Gogny force at distances $r \lesssim 3$ fm (within the interaction range) as well as at larger distances. In the case of $\rho/\rho_0 = 1/8$, for example, this requirement is approximately satisfied if one chooses $e_{\rm cut} = 30$ or 50 MeV; see Fig. 11(b). At $\rho/\rho_0 = 1/512$, a good description of the wave function is obtained with $e_{\rm cut} = 30$ MeV [Fig. 11(c)], and similarly $e_{\rm cut} \sim 70$ MeV is good for the normal density $\rho/\rho_0 = 1$ [Fig. 11(a)]. If one does not include in the comparison the wave function at very short distances $r \lesssim 1$ fm where the repulsion due to the core has influence in the case of the bare force, the constraint on the cutoff energy may be slightly relaxed. For example, at the density $\rho/\rho_0 = 1/512$, the wave functions for $e_{\rm cut} = 30$ and 50 MeV differ by only about $\lesssim$20% at distances $1 < r < 3$ fm, and hence the cutoff energy $e_{\rm cut} = 50$ MeV may also be accepted. Within this tolerance one can choose a value around $e_{\rm cut} \sim 50$ MeV as the cutoff energy, which can be used commonly over the whole density region of interest. This value can be compromised with the constraint $e_{\rm cut} \gtrsim 50$ MeV, which is obtained from the condition on the rms radius of the neutron Cooper pair.

It is interesting to note that cutoff quasiparticle energies around $E_{\rm cut} = 50-70$ MeV have been employed in many recent HFB applications to finite nuclei [9–11,25,28,61,85–88]. These cutoff energies, are consistent with the constraint $e_{\rm cut} \sim 50$ MeV suggested from the above analysis. Much smaller cutoff energies $\lesssim$10 MeV, adopted in early applications of the DDDI [54,55] are not appropriate from the viewpoint of the spatial structure of the neutron Cooper pair wave function. In Ref. [8] the cutoff energy of 20 MeV for the single-particle energy (40 MeV in the center of mass frame

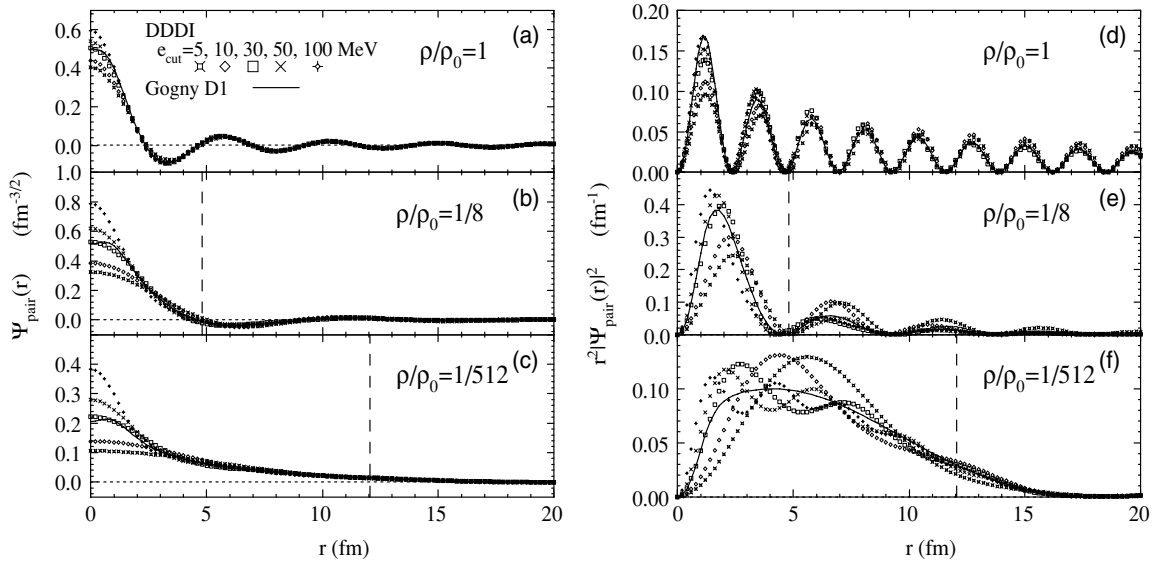

FIG. 11. (a)–(c) Neutron Cooper pair wave function $\Psi_{\rm pair}(r)$ in symmetric nuclear matter calculated with the DDDI having different cutoff energies $e_{\rm cut} = 5, 10, 30, 50, 100$ MeV. The result obtained with the Gogny D1 interaction is shown also by the solid curve. (d)–(f) Same as (a)–(c) but for the probability density $r^2|\Psi_{\rm pair}(r)|^2$.

energy) was shown to describe reasonably the scattering wave function at zero energy. This cutoff energy is not very different from the cutoff energy $e_{\rm cut} \sim 30$ MeV, which is found most reasonable (among the selected examples) in the lowest-density case $\rho/\rho_0 = 1/512$. In the δ interaction model adopted in Ref. [59] the cutoff energy is examined with respect to the low-energy scattering phase shift in the ^1S channel. The cutoff value adopted is around 5–10 MeV in the single-particle energy (9−20 MeV for the center of mass frame energy), in disagreement with our value $e_{\rm cut} \sim 30$ MeV. The difference seems to originate from different strategies to the δ interaction: the momentum dependence of the interaction matrix element is accounted for by the cutoff energy in Ref. [59], while it is taken into account in the present approach mostly through the density-dependent interaction strength $V_0[\rho]$.

C. DDDI parameters

It is useful to parametrize the interaction strength of the DDDI in terms of a simple function of the density. The following form is often assumed [8–11,54,55,58]:

$$V_0[\rho] = v_0 \left(1 - \eta \left(\frac{\rho_{\rm tot}}{\rho_c}\right)^{\alpha}\right), \tag{15}$$

$$\rho_c = 0.16\,{\rm fm}^{-3}, \tag{16}$$

where $\rho_{\rm tot}$ is the total nucleon density. The parameters v_0, η, and α need to be determined. In the works by Bertsch and Esbensen [8] and Garrido *et al.* [58] the parameters are determined so that the parametrized DDDI reproduces the pairing gap obtained with the Gogny force in symmetric nuclear matter as well as the experimental s-wave scattering length at zero density. I shall follow a similar line, but I add the important constraint that the spatial structure of the neutron Cooper pair is also reasonably reproduced. As discussed in the subsection just above, this can be achieved if one constrains the cutoff energy to a value around $e_{\rm cut} \sim 50$ MeV. Note also that the definition of the cutoff energy is different from that in Refs. [8,58], as mentioned in Subsection V A.

The procedure is as follows. I consider symmetric nuclear matter. The cutoff energy is fixed to $e_{\rm cut} = 50$ MeV or 60 MeV for the reasons mentioned above. I then fix the interaction strength $V_0[0] = v_0$ at zero density to a value v_0 that reproduces the scattering length a in the free space; v_0 satisfying this condition is given by [8,58]

$$v_0 = -\frac{2\pi^2\hbar^2 m^{-1}}{k_c - \pi/2a}, \tag{17}$$

$$k_c = \sqrt{2me_{\rm cut}}/\hbar. \tag{18}$$

If one uses as the scattering length a in Eq. (17), the one associated with the Gogny force, the pairing gap of the DDDI in the low-density limit $\rho/\rho_0 \to 0$ coincides with that of the Gogny force. However, since the scattering length $a = -13.5$ fm of the Gogny D1 is slightly off the experimental value, the experimental one, $a = -18.5$ fm, is used for Eq. (17). This is equivalent to constraining the DDDI at the low-density limit by the bare nucleon force.

To determine the other parameters η and α controlling the density dependence of the interaction strength, I first calculate at several representative points of density the values of V_0 with which the neutron gap Δ_F of the Gogny D1 force is reproduced. The parameters η and α are searched so that the simple function Eq. (15) fits well the values of V_0 thus determined. The density interval $\rho/\rho_0 \sim 10^{-2}$−1 ($k_F \sim$ 0.3–1.4 fm^{-1}) is considered in this fitting. The obtained values

TABLE IV. Parameter sets of the density-dependent δ interaction with the cutoff energies $e_{\rm cut} = 50$ and 60 MeV, derived from the procedure applied to the Gogny D1 and D1S, and the G3RS forces. See text for details.

	v_0 [MeV fm^{-3}]	η	α
DDDI-D1			
$e_{\rm cut} = 50$ MeV	−499.9	0.627	0.55
$e_{\rm cut} = 60$ MeV	−458.4	0.603	0.58
DDDI-D1S			
$e_{\rm cut} = 50$ MeV	−499.9	0.652	0.56
$e_{\rm cut} = 60$ MeV	−458.4	0.630	0.60
DDDI-G3RS			
$e_{\rm cut} = 50$ MeV	−499.9	0.872	0.58
$e_{\rm cut} = 60$ MeV	−458.4	0.845	0.59

of the parameters (denoted DDDI-D1) are shown in Table IV, which lists the parameter set obtained with $e_{\rm cut} = 60$ MeV instead of 50 MeV. Another set of the parameters derived in the same way from the Gogny D1S force (DDDI-D1S) is also listed. The same procedure is performed for the G3RS force (DDDI-G3RS).

The pairing gap obtained with these parametrizations of the DDDI are shown in Fig. 12. The resultant gap Δ agrees with that of the corresponding reference gap to the accuracy of about one hundred keV for the whole density region below $\rho/\rho_0 = 1$. Although the results for $e_{\rm cut} = 60$ MeV are not shown here, the agreement with the reference gaps is as good as in the $e_{\rm cut} = 50$ MeV case.

Notice in Table IV that the parameter α takes a similar value, $\alpha = 0.58-0.60$ (in the case $e_{\rm cut} = 60$ MeV) for all of DDDI-D1, DDDI-D1S, and DDDI-G3RS, while the difference between the Gogny forces (DDDI-D1,-D1S) and the G3RS force (DDDI-G3RS) is readily recognized in the value of η. It is also seen that the difference in the cutoff energy slightly influences the values of v_0, η, and α. If one compares the present result with that of Ref. [58], the parameter values $\eta = 0.60-0.63$ for the prefactor and $\alpha = 0.55-0.58$ for the power imply stronger density dependence in $V_0[\rho]$ than that in Ref. [58], where the parameters are determined as $\eta = 0.45$, $\alpha = 0.47$ from a similar fitting to the gap with the Gogny D1 force. This is due to the difference in the cutoff schemes mentioned in Subsection V A. Since the chemical potential μ increases with the density, the energy window measured from the chemical potential μ decreases with increased density in the scheme of Ref. [58], where the cutoff $e(k) < 60$ MeV is adopted for all densities, while in the present cutoff scheme the energy window is kept constant, $e_{\rm cut} = 50, 60$ MeV, independent of the density. Consequently the stronger density dependence in $V_0[\rho]$ is needed in the present case.

It may be interesting to compare the DDDI parameter sets with those determined phenomenologically from the experimental pairing gap in the ground states of finite nuclei. Such a comparison is made in Fig. 13, where the density-dependent interaction strength $V_0[\rho]$ is plotted. The phenomenological DDDI's employed here are the so-called surface and mixed types, for which the prefactor parameter η is fixed to $\eta = 1$ and $\eta = 0.5$, respectively. The power parameter is $\alpha = 1$ for the mixed type [11], while for the surface type $\alpha = 1$ or 1/2 is assumed. (Note that the power parameter in the surface-type DDDI was investigated in Ref. [10], and $1/2 \lesssim \alpha \lesssim 1$ is suggested as a reasonable range of the parameter.) The strength of the surface-type DDDI used here is $v_0 = -521$ MeV fm^{-3} for $\alpha = 1$ and $v_0 = -781$ for $\alpha = 1/2$, taken from Ref. [10], where the value of v_0 is determined by a Skyrme HFB calculation for ^{120}Sn to reproduce the gap 1.25 MeV. The equivalent energy cutoff 60 MeV adopted in the HFB calculation corresponds to our cutoff $e_{\rm cut} = 60$ MeV. In the case of the mixed-type DDDI, the adopted strength

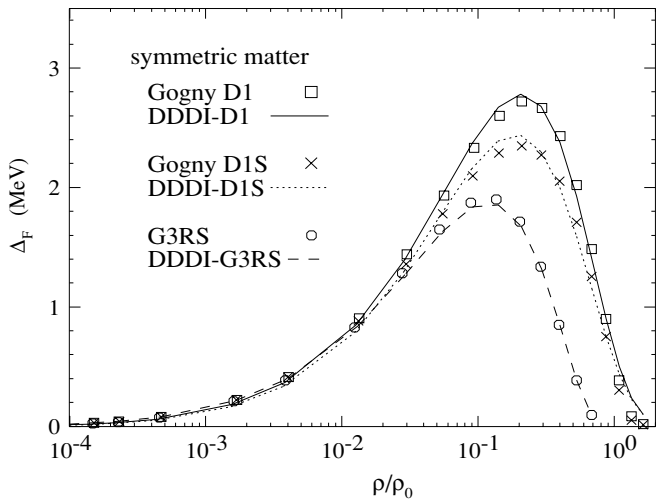

FIG. 12. Pairing gap in symmetric nuclear matter obtained with the DDDI parameter sets shown in Table IV with the cutoff energy $e_{\rm cut} = 50$ MeV. The solid, dotted, and dashed curves represent the result for the parameter sets DDDI-D1, DDDI-D1S, and DDDI-G3RS, respectively. The symbols represent the gap for the reference calculations with the Gogny D1 (square) and D1S (cross) forces, and the G3RS force (circle).

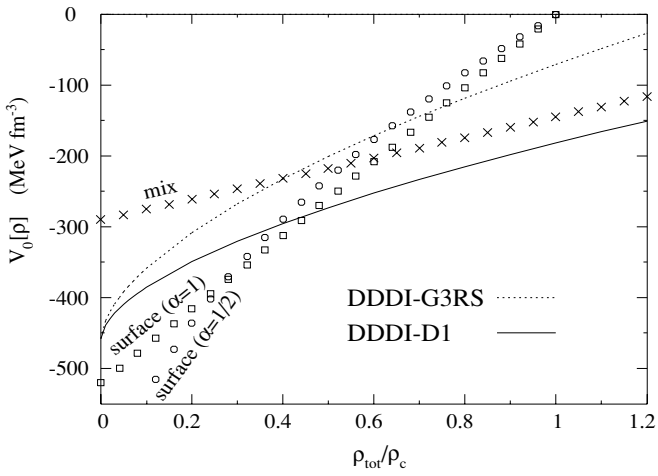

FIG. 13. Density-dependent interaction strength $V_0[\rho]$ of the DDDI for the parameter sets DDDI-D1 (solid curve) and DDDI-G3RS (dotted curve) with $e_{\rm cut} = 60$ MeV. For comparison, $V_0[\rho]$ for the phenomenological DDDI parameters of the surface and mixed types are also shown by the symbols. See the text for details.

is $v_0 = -290$ MeV fm^{-3}, derived from the same condition on ^{120}Sn. It is seen in Fig. 13 that the density dependence in the present parametrizations of $V_0[\rho]$ is mild in the range $\rho_{\rm tot}/\rho_c \gtrsim 0.4$, resembling more that of the mixed-type DDDI than that of the surface type. At lower density, $\rho_{\rm tot}/\rho_c \lesssim 0.3$, the density dependence is stronger than the mixed-type DDDI. Note that the interaction strength $V_0[\rho]$ itself is not large: it takes the values between those of the mixed- and the surface-type DDDI's in this low-density region. The above comparisons suggest that the density dependence in the present parametrization of $V_0[\rho]$ may not be very unrealistic for applications to finite nuclei. It could be also suggested that the present parametrization will be free from the problems pointed out in Ref. [10] for strongly density-dependent DDDI's, such as the surface-type DDDI with small values of the power $\alpha \lesssim 1/2$. For more definite conclusions, one needs to make more quantitative analyses, using the HFB calculation performed directly for finite nuclei. It is also interesting to compare a new approach to the DDDI with microscopically derived cutoff factors [89]. This is, however, beyond the scope of this paper, and such analyses will be pursued in future.

VI. CONCLUSIONS

I have analyzed the spatial structure of the neutron Cooper pair obtained with the BCS approximation for neutron and symmetric nuclear matter by using a bare force and the effective Gogny interaction. The size of the Cooper pair varies significantly with the density: its rms radius $\xi_{\rm rms}$ becomes as small as $\sim$5 fm around $\rho/\rho_0 \approx 10^{-2}-0.2$, and $\xi_{\rm rms}$ smaller than the average interneutron distance d is realized over a very wide range, $\rho/\rho_0 \approx 10^{-4}-0.1$, at low density. The analysis of the Cooper pair wave function indicates that the probability for the spin up and down neutrons in the pair to be correlated within the average interneutron distance d exceeds 0.8 in this density range. The strong spatial correlation at short relative distances is also seen for the modest density $\rho/\rho_0 \sim 0.5$, at which the concentration of the pair neutrons within the interaction range $\sim$3 fm reaches about 0.5. These observations suggest that the spatial dineutron correlation is strong, at least in the level of the mean-field approximation, in low-density superfluid uniform matter over the wide range of densities $\rho/\rho_0 \approx 10^{-4}-0.5$. The essential feature does not depend on the interactions.

The behavior of the strong dineutron correlation have been investigated in connection with the crossover phenomenon between the conventional pairing of the weak coupling BCS type and the Bose-Einstein condensation of the bound neutron pairs. From the comparison with the analytic BCS-BEC crossover model, it is found that the density region $\rho/\rho_0 \approx 10^{-4}-10^{-1}$ corresponds to the domain of the BCS-BEC crossover.

I have also examined how the density-dependent δ interaction (DDDI) combined with a finite cutoff energy can describe the spatial correlation of the neutron Cooper pair. The spatial correlation at short relative distances and the rms radius of the pair are described consistently over a wide density region $0 < \rho/\rho_0 \lesssim 1$, provided that one adopts a cutoff energy around $e_{\rm cut} \sim 50$ MeV defined with respect to the chemical potential. I have derived a possible parametrization of the DDDI, which satisfies this new condition on top of the constraints on the gap in symmetric nuclear matter and on the scattering length in the free space. The new DDDI parametrizations may be consistent with or at least not strongly contradictory to the phenomenological DDDI's derived from the gap in finite nuclei.

ACKNOWLEDGMENTS

The author thanks P. Schuck and M. Hjorth-Jensen for useful discussions. He also thanks the Yukawa Institute for Theoretical Physics at Kyoto University and the Institute for Nuclear Theory at University of Washington. Discussions during the YITP workshop YITP-W-05-01 on "New Developments in Nuclear Self-Consistent Mean-Field Theories" and the INT workshop "Towards a Universal Density Functional for Nuclei" in the program INT-05-3 "Nuclear Structure Near the Limits of Stability" were useful in completing this work. Discussions with the members of the Japan-U.S. Cooperative Science Program, "Mean-Field Approach to Collective Excitations in Unstable Medium-Mass and Heavy Nuclei" are also acknowledged. This work was supported by a Grant-in-Aid for Scientific Research (17540244) from the Japan Society for the Promotion of Science.

[1] A. Bohr and B. R. Mottelson, *Nuclear Structure* (Benjamin, New York, 1975), Vol. II.
[2] Y. R. Shimizu, J. D. Garrett, R. A. Broglia, M. Gallardo, and E. Vigezzi, Rev. Mod. Phys. **61**, 131 (1989).
[3] T. Takatsuka and R. Tamagaki, Prog. Theor. Phys. Suppl. **112**, 27 (1993).
[4] U. Lombardo and H.-J. Schulze, in *Physics of Neutron Star Interiors*, edited by D. Blaschke, N. K. Glendenning, and A. Sedrakian, Vol. 578 of Lecture Notes in Physics (Springer, New York, 2001), p. 30.
[5] D. J. Dean and M. Hjorth-Jensen, Rev. Mod. Phys. **75**, 607 (2003).
[6] H. Heiselberg and V. Pandharipande, Annu. Rev. Nucl. Part. Sci. **50**, 481 (2000).
[7] D. G. Yakovlev and C. J. Pethick, Annu. Rev. Astron. Astrophys. **42**, 169 (2004).
[8] G. F. Bertsch and H. Esbensen, Ann. Phys. (N.Y.) **209**, 327 (1991).
[9] J. Dobaczewski, W. Nazarewicz, T. R. Werner, J. F. Berger, C. R. Chinn, and J. Dechargé, Phys. Rev. C **53**, 2809 (1996).
[10] J. Dobaczewski, W. Nazarewicz, and P.-G. Reinhard, Nucl. Phys. **A693**, 361 (2001).
[11] J. Dobaczewski and W. Nazarewicz, Prog. Theor. Phys. Suppl. **146**, 70 (2002); J. Dobaczewski, W. Nazarewicz, and M. V. Stoitsov, Eur. Phys. J. A **15**, 21 (2002).
[12] I. Tanihata, H. Hamagaki, O. Hashimoto, Y. Shida, N. Yoshikawa, K. Sugimoto, O. Yamakawa, T. Kobayashi, and N. Takahashi, Phys. Rev. Lett. **55**, 2676 (1985).

[13] I. Tanihata, T. Kobayashi, T. Suzuki, K. Yoshida, S. Shimoura, K. Sugimoto, K. Matsuta, T. Minamisono, W. Christe, D. Olson, and H. Wieman, Phys. Lett. **B287**, 307 (1992).
[14] A. Ozawa, O. Bochkarev, L. Chulkov, D. Cortina, H. Geissel, M. Hellström, M. Ivanov, R. Janik, K. Kimura, T. Kobayashi, A. A. Korsheninnikov, G. Münzenberg, F. Nickel, Y. Ogawa, A. A. Ogloblin, M. Pfützner, V. Pribora, H. Simon, B. Sitár, P. Strmend, K. Sümmerer, T. Suzuki, I. Tanihata, M. Winkler, and K. Yoshida, Nucl. Phys. **A691**, 599 (2001).
[15] P. G. Hansen and B. Jonson, Europhys. Lett. **4**, 409 (1987).
[16] K. Ikeda, INS Report JHP-7, 1988 (in Japanese; unpublished); Nucl. Phys. **A538**, 355c (1992).
[17] M. V. Zhukov, B. V. Danilin, D. V. Fedorov, J. M. Bang, I. J. Thompson, and J. S. Vaagen, Phys. Rep. **231**, 151 (1993).
[18] F. Barranco, P. F. Bortignon, R. A. Broglia, G. Coló, and E. Vigezzi, Eur. Phys. J. A **11**, 385 (2001).
[19] S. Aoyama, K. Katō, and K. Ikeda, Prog. Theor. Phys. Suppl. **142**, 35 (2001); T. Myo, S. Aoyama, K. Katō, and K. Ikeda, Prog. Theor. Phys. **108**, 133 (2002).
[20] K. Hagino and H. Sagawa, Phys. Rev. C **72**, 044321 (2005).
[21] D. Sackett, K. Ieki, A. Galonsky, C. A. Bertulani, H. Esbensen, J. J. Kruse, W. G. Lynch, D. J. Morrissey, N. A. Orr, B. M. Sherrill, H. Schulz, A. Sustich, J. A. Winger, F. Deák, Á. Horváth, Á. Kiss, Z. Seres, J. J. Kolata, R. E. Warner, and D. L. Humphrey, Phys. Rev. C **48**, 118 (1993).
[22] S. Shimoura, T. Nakamura, M. Ishihara, N. Inabe, T. Kobayashi, T. Kubo, R. H. Siemssen, I. Tanihata, and Y. Watanabe, Phys. Lett. **B348**, 29 (1995).
[23] M. Zinser, F. Humbert, T. Nilsson, W. Schwab, H. Simon, T. Aumann, M. J. G. Borge, L. V. Chulkov, J. Cub, Th. W. Elze, H. Emling, H. Geissel, D. Guillemaud-Mueller, P. G. Hansen, R. Holzmann, H. Irnich, B. Jonson, J. V. Kratz, R. Kulessa, Y. Leifels, H. Lenske, A. Magel, A. C. Mueller, G. Münzenberg, F. Nickel, G. Nyman, A. Richter, K. Riisager, C. Scheidenberger, G. Schrieder, K. Stelzer, J. Stroth, A. Surowiec, O. Tengblad, E. Wajda, and E. Zude, Nucl. Phys. **A619**, 151 (1997).
[24] K. Ieki, A. Galonsky, D. Sackett, J. J. Kruse, W. G. Lynch, D. J. Morrissey, N. A. Orr, B. M. Sherrill, J. A. Winger, F. Deák, Á. Horváth, Á. Kiss, Z. Seres, J. J. Kolata, R. E. Warner, and D. L. Humphrey, Phys. Rev. C **54**, 1589 (1996).
[25] M. Matsuo, K. Mizuyama, and Y. Serizawa, Phys. Rev. C **71**, 064326 (2005).
[26] P. Ring and P. Schuck, *The Nuclear Many-Body Problem* (Springer-Verlag, New York, 1980).
[27] J. -P. Blaizot and G. Ripka, *Quantum Theory of Finite Systems* (MIT Press, Cambridge, Mass., 1986).
[28] J. Dobaczewski, H. Flocard, and J. Treiner, Nucl. Phys. **A422**, 103 (1984).
[29] A. Bulgac, preprint Report FT-194-1980, arXiv:nucl-th/9907088.
[30] A. J. Leggett, in *Modern Trends in the Theory of Condensed Matter*, edited by A. Pekalski and R. Przystawa, Vol. 115 of Lecture Note in Physics (Springer-Verlag, Berlin, 1980); J. Phys. (Paris) **41**, C7–19 (1980).
[31] P. Nozières and S. Schmitt-Rink, J. Low Temp. Phys. **59**, 195 (1985).
[32] J. Bardeen, L. N. Cooper, and J. R. Schrieffer, Phys. Rev. **108**, 1175 (1957); P. G. de Gennes, *Superconductivity of Metals and Alloys* (Benjamin, New York, 1966); M. Tinkham, *Introduction to Superconductivity* (McGraw-Hill, New York, 1975).
[33] C. A. R. Sá de Melo, M. Randeria, and J. R. Engelbrecht, Phys. Rev. Lett. **71**, 3202 (1993).
[34] J. R. Engelbrecht, M. Randeria, and C. A. R. Sá de Melo, Phys. Rev. B **55**, 15153 (1997).
[35] M. Randeria, in *Bose-Einstein Condensation*, edited by A. Griffin, D. Snoke, and S. Stringari (Cambridge Univ. Press, Cambridge, U.K., 1995).
[36] C. A. Regal, M. Greiner, and D. S. Jin, Phys. Rev. Lett. **92**, 040403 (2004).
[37] T. Alm, B. L. Friman, G. Röpke, and H. Schulz, Nucl. Phys. **A551**, 45 (1993).
[38] H. Stein, A. Schnell, T. Alm, and G. Röpke, Z. Phys. A **351**, 295 (1995).
[39] M. Baldo, U. Lombardo, and P. Schuck, Phys. Rev. C **52**, 975 (1995).
[40] U. Lombardo and P. Schuck, Phys. Rev. C **63**, 038201 (2001).
[41] U. Lombardo, P. Nozières, P. Schuck, H.-J. Schulze, and A. Sedrakian, Phys. Rev. C **64**, 064314 (2001).
[42] T. Takatsuka, Prog. Theor. Phys. **48**, 1517 (1972).
[43] T. Takatsuka, Prog. Theor. Phys. **71**, 1432 (1984).
[44] M. Baldo, J. Cugnon, A. Lejeune, and U. Lombardo, Nucl. Phys. **A515**, 409 (1990).
[45] Ø. Elgarøy, L. Engvik, M. Hjorth-Jensen, and E. Osnes, Nucl. Phys. **A604**, 466 (1996).
[46] V. A. Khodel, V. V. Khodel, and J. W. Clark, Nucl. Phys. **598**, 390 (1996).
[47] F. V. De Blasio, M. Hjorth-Jensen, Ø. Elgarøy, L. Engvik, G. Lazzari, M. Baldo, and H.-J. Schulze, Phys. Rev. C **56**, 2332 (1997).
[48] M. Serra, A. Rummel, and P. Ring, Phys. Rev. C **65**, 014304 (2001).
[49] E. Garrido, P. Sarriguren, E. Moya de Guerra, U. Lombardo, P. Schuck, and H. J. Schulze, Phys. Rev. C **63**, 037304 (2001).
[50] H. Kucharek, P. Ring, P. Schuck, R. Bengtsson, and M. Girod, Phys. Lett. **B216**, 249 (1989); H. Kucharek, P. Ring, and P. Schuck, Z. Phys. A **334**, 119 (1989).
[51] A. Sedrakian, T. T. S. Kuo, H. Müther, and P. Schuck, Phys. Lett. **B576**, 68 (2003).
[52] J. Dechargé and D. Gogny, Phys. Rev. C **21**, 1568 (1980).
[53] R. R. Chasman, Phys. Rev. C **14**, 1935 (1976).
[54] J. Terasaki, P.-H. Heenen, P. Bonche, J. Dobaczewski, and H. Flocard, Nucl. Phys. **A593**, 1 (1995).
[55] N. Tajima, P. Bonche, H. Flocard, P.-H. Heenen, M. S. Weiss, Nucl. Phys. **A551**, 434 (1993).
[56] S. A. Fayans and D. Zawischa, Phys. Lett. **B383**, 19 (1996).
[57] S. A. Fayans, S. V. Tolokonnikov, E. L. Trykov, and D. Zawischa, Nucl. Phys. **A676**, 49 (2000).
[58] E. Garrido, P. Sarriguren, E. Moya de Guerra, and P. Schuck, Phys. Rev. C **60**, 064312 (1999).
[59] H. Esbensen, G. F. Bertsch, and K. Hencken, Phys. Rev. C **56**, 3054 (1997).
[60] A. Bulgac and Y. Yu, Phys. Rev. Lett. **88**, 042504 (2002); A. Bulgac, Phys. Rev. C **65**, 051305(R) (2002).
[61] Y. Yu and A. Bulgac, Phys. Rev. Lett. **90**, 222501 (2003).
[62] M. Matsuo, Y. Serizawa, and K. Mizuyama, J. Phys. Conf. Ser. **20**, 113 (2005); M. Matsuo, "Proceedings of the YITP workshop New Developments in Nuclear Self-Consistent Mean-Field Theories," Soryushiron Kenkyu **112**, B59 (2005).
[63] R. Tamagaki, Prog. Theor. Phys. **39**, 91 (1968).
[64] G. F. de Téramond and B. Gabioud, Phys. Rev. C **36**, 691 (1987).

[65] J. F. Berger, M. Girod, and D. Gogny, Comput. Phys. Commun. **63**, 365 (1991).
[66] J. M. C. Chen, J. W. Clark, E. Krotscheck, and R. A. Smith, Nucl. Phys. **A451**, 509 (1986).
[67] J. M. C. Chen, J. W. Clark, R. D. Davé, and V. V. Khodel, Nucl. Phys. **A555**, 59 (1993).
[68] T. L. Ainsworth, J. Wambach, and D. Pines, Phys. Lett. **B222**, 173 (1989).
[69] J. Wambach, T. L. Ainsworth, and D. Pines, Nucl. Phys. **A555**, 128 (1993).
[70] H.-J. Schulze, J. Cugnon, A. Lejeune, M. Baldo, and U. Lombardo, Phys. Lett. **B375**, 1 (1996).
[71] H.-J. Schulze, A. Polls, and A. Ramos, Phys. Rev. C **63**, 044310 (2001).
[72] U. Lombardo, P. Schuck, and W. Zuo, Phys. Rev. C **64**, 021301(R) (2001).
[73] C. Shen, U. Lombardo, P. Schuck, W. Zuo, and N. Sandulescu, Phys. Rev. C **67**, 061302(R) (2003).
[74] A. Schwenk, B. Friman, and G. E. Brown, Nucl. Phys. **A713**, 191 (2003).
[75] U. Lombardo, P. Schuck, and C. Shen, Nucl. Phys. **A731**, 392 (2004).
[76] H. Heiselberg, C. J. Pethick, H. Smith, and L. Viverit, Phys. Rev. Lett. **85**, 2418 (2000).
[77] A. Fabrocini, S. Fantoni, A. Y. Illarionov, and K. E. Schmidt, Phys. Rev. Lett. **95**, 192501 (2005).
[78] F. Barranco, R. A. Broglia, G. Gori, E. Vigezzi, P. F. Bortignon, and J. Terasaki, Phys. Rev. Lett. **83**, 2147 (1999).
[79] J. Terasaki, F. Barranco, R. A. Broglia, E. Vigezzi, and P. F. Bortignon, Nucl. Phys. **A697**, 127 (2002).
[80] G. Gori, F. Ramponi, F. Barranco, P. F. Bortignon, R. A. Broglia, G. Colò, and E. Vigezzi, Phys. Rev. C **72**, 011302(R) (2005).
[81] Ø. Elgarøy and M. Hjorth-Jensen, Phys. Rev. C **57**, 1174 (1998).
[82] M. Marini, F. Pistolesi, and G. C. Strinati, Eur. Phys. J. B **1**, 151 (1998).
[83] T. Papenbrock and G. F. Bertsch, Phys. Rev. C **59**, 2052 (1999).
[84] H. Heiselberg, Phys. Rev. A **63**, 043606 (2001).
[85] M. Grasso, N. Sandulescu, N. V. Giai, and R. J. Liotta, Phys. Rev. C **64**, 064321 (2001).
[86] M. V. Stoitsov, J. Dobaczewski, W. Nazarewicz, S. Pittel, and D. J. Dean, Phys. Rev. C **68**, 054312 (2003).
[87] E. Terán, V. E. Oberacker, and A. S. Umar, Phys. Rev. C **67**, 064314 (2003).
[88] M. Bender, P.-H. Heenen, and P.-G. Reinhard, Rev. Mod. Phys. **75**, 121 (2003).
[89] T. Duguet, Phys. Rev. C **69**, 054317 (2004).